

Ce_{0.8}Y_{0.2}O_{2-δ} — EFFECT OF PRODUCTION METHOD ON STRUCTURE AND ELECTROPHYSICAL PROPERTIES

I. V. Sudzhanskaya,¹ A. E. Vasil'ev,¹ M. N. Yapryntsev,¹ Yu. S. Nekrasova,² and A. N. Oleinik¹

Translated from *Steklo i Keramika*, No. 8, pp. 43–51, August, 2022.

Original article submitted April 25, 2022.

The solid solution Ce_{0.8}Y_{0.2}O_{2-δ} was obtained by three methods: sol-gel, glycine-nitrate, and solid-phase reactions. The synthesis temperature was 1350°C for the sol-gel method and 1500°C for the remaining samples. The x-ray method showed that all samples have a cubic lattice with fluorite structure. The microstructure, density, electrical conductivity, microhardness, and crack resistance of the resulting ceramics were studied. It was found by means of impedance spectroscopy that the Ce_{0.8}Y_{0.2}O_{2-δ} system obtained by the sol-gel method has the highest electrical conductivity, 5.37 mS/cm at 550°C, and the lowest activation energy, equal to 0.83 eV in the temperature range of 300–550°C. The contribution made to the conductivity by grains and grain boundaries is determined. It is shown that the total conductivity for all samples decreases due to the resistance along the grain boundaries.

Keywords: doped cerium, ion conductivity, impedance spectroscopy, microhardness, crack resistance.

INTRODUCTION

The CeO₂-based solid solution with fluorite structure is characterized by high ionic conductivity at lower temperatures than yttrium-stabilized zirconium and by the absence of phase transitions at temperatures ranging from room to melting point, which makes it promising for use in low- and medium-temperature solid electrolytes of solid oxide fuel cells (SOFC) [1–8], semiconductor heterostructures [9], oxygen sensors [10–12], in nanostructured materials in the energy sector [13], and catalysts [14–15] as well as in the design of micro-SOFC as a solid electrolyte for battery replacement in small electronic devices such as laptops, cell phones, and elsewhere [16–19].

The electric conductivity of CeO₂ ceramics can be increased by introducing Sm, Gd, and Y impurities [4, 6, 8, 11, 14, 20–23].

The electric conductivity of electrolytes is determined by the density of sintered ceramic materials, impurity type, impurity concentration, and grain boundaries [24–28]. However, the question of the influence of the method of obtaining

a ceramic system based on CeO₂ on the structure and electro-physical properties remains open.

It is known that among the methods used to for obtaining ceramic systems, the most popular are: the reaction method in the solid phase [29] as the simplest, cheapest, and fastest; sol-gel method [30], since it allows making powders with the highest homogeneity, as a result of which denser ceramics are formed during sintering; glycine-nitrate method [29] as a fairly simple way to obtain a finer powder.

The solid solution Y₂O₃–CeO₂ is of particular interest because up to 700°C its electrical conductivity is relatively high [21, 31, 32] and the yttrium element is cheap [33].

The purpose of the present work is to determine how the method of obtaining ceramics affects the structure and electrical properties of the composition 0.2Y₂O₃–0.8CeO₂ as an example.

EXPERIMENTAL RESULTS

Sample preparation

Powders of the composition (stoichiometric) 0.8CeO₂–0.2Y₂O₃ were obtained by three methods: solid-phase reactions (SPR), sol-gel (SG), and glycine-nitrate (GN). Y(NO₃)₃·6H₂O 99.9% (Acros organics) and

¹ Belgorod National Research University, Belgorod, Russia (e-mail: sudzhanskaya@bsu.edu.ru).

² V. G. Shukhov Belgorod State Technological University, Belgorod, Russia (e-mail: yulia_nekrasova@mail.ru).

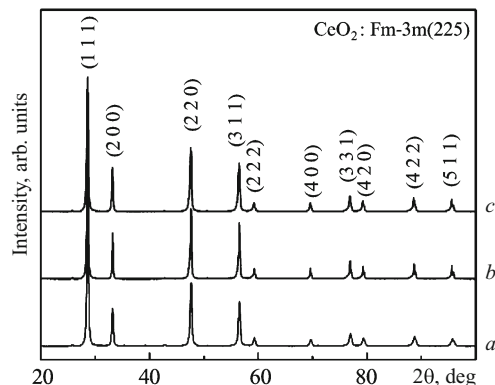


Fig. 1. X-ray diffraction pattern of ceramic samples of the system $\text{Ce}_{0.8}\text{Y}_{0.2}\text{O}_{2-\delta}$ obtained by different methods: a) SG; b) GN; c) SPR.

$\text{Ce}(\text{NO}_3)_3 \cdot 6\text{H}_2\text{O}$ 99.5% (Acros organics) were used as precursors.

Reaction in the solid phase method. CeO_2 and Y_2O_3 precursors were obtained by annealing at 600°C for 1 h in air until the required phase is formed. Stoichiometric powders were stirred in an agate mortar for 1 h with the addition of ethyl alcohol; the resulting suspension was dried at 373 K for 1 h.

Sol-gel method. For synthesis by the sol-gel method, the precursors $\text{Y}(\text{NO}_3)_3 \cdot 6\text{H}_2\text{O}$ and $\text{Ce}(\text{NO}_3)_3 \cdot 6\text{H}_2\text{O}$ are taken according to stoichiometry in accordance with the composition $\text{Ce}_{0.8}\text{Y}_{0.2}\text{O}_{2-\delta}$. The precursors are dissolved in 100 ml of water in a beaker until a clear solution is formed (with constant stirring and at 50°C). The resulting solution is kept for 1 h at 50°C . Next, 35 ml of a 25% aqueous ammonia solution is added. The resulting gel is kept at room temperature for 1 day. Water removal is conducted at 125°C for several hours. After drying, the gel is annealed at 600°C for 1 h until the required phase is formed.

Glycine-nitrate method. Yttrium and cerium nitrates were also used for the synthesis by the glycine-nitrate method. Glycine was taken as a ‘fuel’ in molar ratio 1 : 1 to nitrate ions.

Weighed portions of yttrium and cerium nitrates were weighed into a flat-bottomed flask with a wide neck. They are dissolved at low heat (50°C) in a minimum amount of water. Glycine is added to the resulting solution. The solution is allowed to stand for 30 min until the glycine is completely dissolved.

The resulting solution is slowly evaporated until the mixture starts to ignite. The resulting flaky powder was thoroughly ground in a mortar and annealed in a muffle furnace at 600°C for 1 h to remove traces of carbon.

The powders were compacted by biaxial isostatic pressing at 250 MPa into tablets. The sintering temperature was determined based on the analysis of the literature [21] and amounted to 1500°C in an air atmosphere for 1 h, after which the samples obtained by the sol-gel method completely melted, which is associated with the smallest grain size compared to other methods and is confirmed by the SEM images displayed in Fig. 2. The sintering temperature of the ceramics obtained by the sol-gel method was determined via TGA/DSC analysis, from which the sintering temperature was found to be 1350°C .

Equipment and procedures

A Rigaku Ultima IV x-ray diffractometer was employed to determine the phase composition of the obtained samples. A Quanta 200 3D scanning ion-electron microscope was used to investigate the microstructure. A Novocontrol Concept 43 impedance meter with alternating current was used for impedance spectroscopy at temperatures ranging from room temperature to 800°C and frequencies 0.1 Hz to 1 MHz. Silver paste was applied beforehand to the end faces of the tablets on both sides. The measurement was performed with platinum electrodes. The density of the obtained samples after sintering was determined by pycnometry using a micrometrics AccuPyc II 1340 helium pycnometer; 15 measurements were performed for each sample. The mean value was fixed as the result. The microhardness and crack resistance of ceramic systems were investigated with a DM-8 microhardness tester, making 10 imprints for each sample. The load on the indenter was equal to 0.1 kg, and the pene-

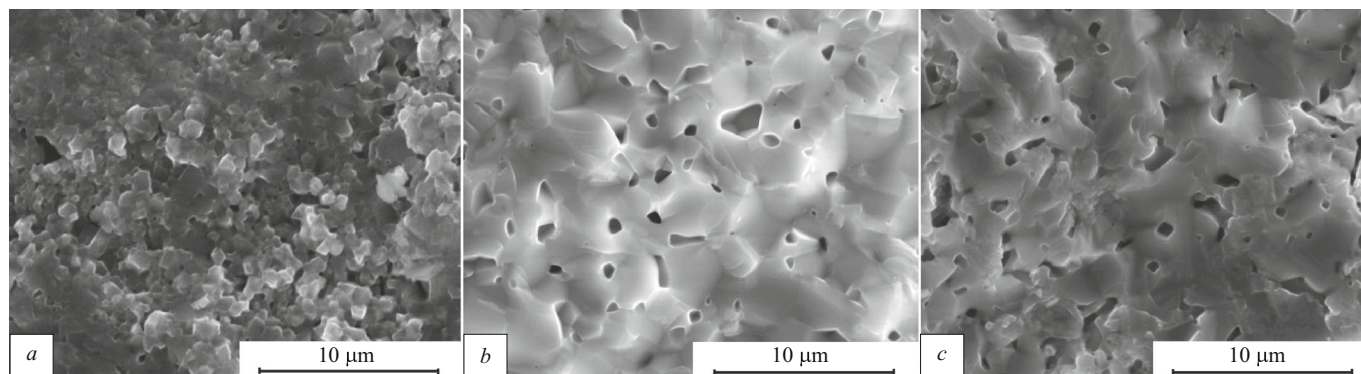


Fig. 2. SEM images of the cleavage of samples obtained by different methods: a) SG; b) GN; c) SPR.

tration time of the indenter into the surface of the material was equal to 15 sec. The arithmetic mean of 10 measurements was taken as the result.

RESULTS AND DISCUSSION

Microstructure characteristics

A diffraction pattern obtained for the system Ce_{0.8}Y_{0.2}O_{2-δ} by different methods — SG, GN, SPR — is displayed in Fig. 1; it is identical for all three methods.

Post-sintering XRD analysis of the samples shows that a cubic phase with a fluorite structure (space group of symmetry *Fm3m*) obtains for all three methods of preparing powders with lattice parameters $a = b = c = 5.4019 \text{ \AA}$.

The post-sintering density of the samples is equal to 6.03 g/cm³ for the SPR method, 6.47 g/cm³ for the GN method, and 6.51 g/cm³ for the SG method.

SEM images of the cleavage of Ce_{0.8}Y_{0.2}O_{2-δ} samples obtained by different methods are shown in Fig. 2. The smallest grain size and the greatest homogeneity are seen in the ceramic, obtained by SG (Fig. 2a), with average grain size 0.4 μm, which is associated with a lower sintering temperature. For GN and SPR, this characteristic is equal to 2.86 and 2.62 μm (Fig. 2b and c), respectively.

Impedance spectroscopy and specific electric conductivity

Impedance spectroscopy was used to measure the total resistance R_t of Ce_{0.8}Y_{0.2}O_{2-δ} ceramic electrolytes. The total resistance R_t is the sum of the bulk R_b and intergranular R_{gb} resistance

$$R_t = R_b + R_{gb}. \quad (1)$$

The values of the total resistance were used to calculate the total ionic conductivity of the sintered samples according to the expression

$$\sigma_t = \frac{l}{R_t A}, \quad (2)$$

where l is the sample thickness and A is the area of a tablet.

The conductivity of the volume of the grains and grain boundaries was determined by the formulas [34]:

$$\sigma_b = \frac{l}{R_b A}; \quad \sigma_{gb} = \frac{l}{R_{gb} A}.$$

The contribution of the bulk and intergranular resistances to the total resistance can be determined by using the capacitances in the impedance spectra. Ideally, the frequency response of polycrystalline doped cerium oxide can be simulated by connecting a resistor and a capacitor with losses RC in parallel. In the case under consideration the microstructure of the samples is inhomogeneous, so that the lossy capacitor was replaced by a constant phase Q element. The equivalent

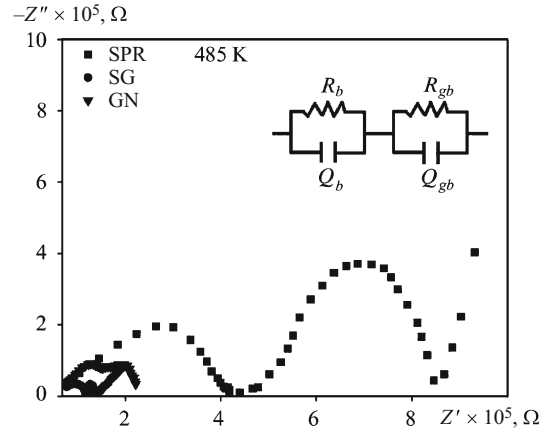


Fig. 3. Impedance spectrum of the solid solution Ce_{0.8}Y_{0.2}O_{2-δ}, obtained by different methods, at a temperature 485 K: 1) SG; 2) GN; 3) SPR.

circuits containing two serially connected subcircuits with a constant phase element, resistance along the volume of the grains and resistance along the grain boundaries, are presented in the inset in Fig. 3.

The impedance spectrum of the Ce_{0.8}Y_{0.2}O_{2-δ} samples plotted in the Nyquist coordinates is shown in Fig. 3.

A block model [35] was used to analyze the impedance spectra. The choice of the impedance temperature is determined by the possibility of estimating the contribution of the grain volume and grain boundaries to the total resistance. With an increase in temperature the relaxation frequency of polarization processes increases, which leads to a shift of the corresponding arcs to higher frequencies. Since the frequency range in the equipment is limited, not all arcs are observed as temperature rises.

The Nyquist plots constructed to determine the contribution of the volume of grains and grain boundaries to the resistance show that three relaxation processes are observed for the samples of Ce_{0.8}Y_{0.2}O_{2-δ} ceramics obtained by the SG and SPR methods: a high-frequency arc associated with the transport of oxygen inside the grain volume; medium-frequency arc associated with conduction along grain boundaries; an increase in the low-frequency region due to the movement of oxygen ions in a concentration gradient near the solid electrolyte–electrode interface. The impedance spectrum of the Ce_{0.8}Y_{0.2}O_{2-δ} solid solution obtained by the GN method has two circles, indicating the contribution of the volume of grains and their boundaries to the total conductivity of the material. The third section, associated with the influence of the electrodes, is situated at lower frequencies. The frequency dependence of the electrical conductivity of the Ce_{0.8}Y_{0.2}O_{2-δ} system, obtained by different methods, is shown in Fig. 4.

Comparing the methods for obtaining Ce_{0.8}Y_{0.2}O_{2-δ} ceramics based on the analysis of isotherms of the frequency response of electrical conductivity and impedance results, it can be concluded that GN-ceramics with the highest material

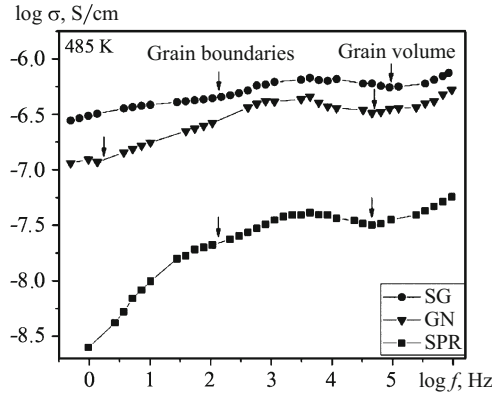


Fig. 4. Spectrum of the frequency dependence of the electrical conductivity of the solid solution $\text{Ce}_{0.8}\text{Y}_{0.2}\text{O}_{2-\delta}$ obtained by the SG, GN, SPR methods at 485 K.

density and the smallest grain size have the highest electrical conductivity. This is associated with the lowest sintering temperature.

The highest electrical conductivity of samples sintered at a lower temperature is due to a lower concentration of impurities at the grain boundaries as a result of small grain size and large grain boundary areas, as well as less solute segregation and less developed space charge regions at grain boundaries due to small grain size and low mobility of cations at lower temperatures [31].

To determine the transport properties of solid electrolytes, the temperature dependence of the total, grain, and grain-boundary electrical conductivity of the ceramics $\text{Ce}_{0.8}\text{Y}_{0.2}\text{O}_{2-\delta}$ ceramics was constructed in the $\ln \sigma(1/T)$ coordinates. According to the Arrhenius law (3)

$$\sigma = \sigma_0 \exp(-E/(kT)), \quad (3)$$

where σ_0 is the pre-exponential factor; E is the activation energy of electrical conductivity; k is the Boltzmann con-

stant, equal to 1.3810^{-23} J/K. The results are presented in Fig. 5.

The total activation energy of the conduction process in the ceramics $\text{Ce}_{0.8}\text{Y}_{0.2}\text{O}_{2-\delta}$, calculated from the slope of the linear dependence $\ln \sigma(1/T)$ (Fig. 5a) was equal to 0.83 eV for the SG method, 0.86 eV for GN, and 1.03 eV for SPR, which is consistent with the results presented in [21]. The total conductivity at 550°C was 5.37 mS/cm for the SG method, 4.10 mS/cm for GN, and 0.58 mS/cm for SPR.

The values of the activation energy of the conduction process in the grain bulk and along grain boundaries (Fig. 5b) and the total electrical conductivity are presented in Table 1.

It follows from the plot in Fig. 5b and Table 1 that the highest electrical conductivity obtains in the system $\text{Ce}_{0.8}\text{Y}_{0.2}\text{O}_{2-\delta}$ obtained by the SG method.

For all three methods of obtaining an electrolyte, the conductivity of grains is higher than the conductivity of grain boundaries in the entire temperature range, i.e. the total conductivity decreases on account of grain boundary conduction. The grain boundary conductivity is determined by a grain blocking factor. The degree of blocking of grain boundaries for the transport of oxygen ions is determined by the blocking factor [36, 37]

$$\alpha_{gb} = \frac{R_{gb}}{(R_b + R_{gb})}. \quad (4)$$

The blocking factor carries information about the proportion of charge carriers that are partially blocked at internal interfaces with respect to the total amount of electric charge carriers [37]. The values of the blocking factor are given in Table 2 for all obtained samples.

The $\text{Ce}_{0.8}\text{Y}_{0.2}\text{O}_{2-\delta}$ system obtained by the SG method has the lowest value of the blocking factor and SPR the highest. This agrees with the conduction results. For all samples the blocking factor decreases with rising temperature; this is due

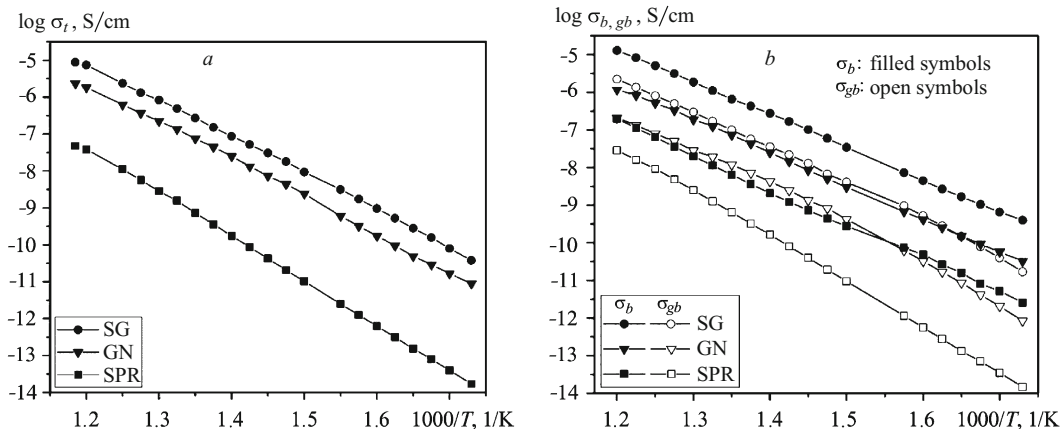


Fig. 5. Logarithmic dependence of the total electrical conductivity (a), electrical conductivity in the grain bulk and along grain boundaries (b) on the value of the reciprocal temperature of the $\text{Ce}_{0.8}\text{Y}_{0.2}\text{O}_{2-\delta}$ ceramic obtained by the SG, GN, and SPR methods, frequency equals to 1.13 kHz.

TABLE 1. Values of the Total, Grain Boundary, and Grain Activation Energies of the System Ce_{0.8}Y_{0.2}O_{2-δ} Depending on the Preparation Method and Total Electrical Conductivity at 550°C.

Method	$\sigma_t, 10^{-3} \text{ Sm/cm,}$ 550°C	$E_t, \text{ eV,}$ 300 – 550°C	$E_b, \text{ eV,}$ 300 – 550°C	$E_{gb}, \text{ eV,}$ 300 – 550°C
SG	5.37	0.83	0.73	0.85
GN	4.10	0.86	0.74	0.88
SPR	0.58	1.03	0.80	1.03

to an increase in thermal activation processes, as a result of which complex associates of defect are destroyed, releasing a larger number of charge carriers involved in the hopping mechanism.

The Ce_{0.8}Y_{0.2}O_{2-δ} system obtained by the SG method with a higher density and small grain size exhibits a much higher grain boundary conductivity because the grain boundary area is so large that the final amount of impurities contained in these samples, such as Si, is insufficient for a continuous and homogeneous layer of the glassy phase to form along the grain boundaries. As a result, grain boundary zones remain without impurities for contact with the grain. Consequently, oxygen ions move through impurity-free boundaries [31].

Mechanical properties

The Vickers microhardness and the fracture toughness were measured to reckon the influence of the preparation method on the mechanical properties of the system Ce_{0.8}Y_{0.2}O_{2-δ}. The results of [38] were used to reckon the fracture toughness:

$$K_{1c} = 0.203(c/a)^{-3/2} \text{ Ha}^{1/2}, \tag{5}$$

where *a* is the length of the indentation diagonal, mm; *c* — the crack length, mm; H — the Vickers hardness (Hv).

The measurements of microhardness and fracture toughness of ceramic Ce_{0.8}Y_{0.2}O_{2-δ} are presented in Table 3.

The highest hardness and fracture toughness 11.56 GPa and 2.29 MPa · m^{1/2} were demonstrated by the solid solution obtained by the SG method; the microhardness was equal

TABLE 2. Blocking Factor α_{gb} for All Samples at Different Temperatures

Sample production method	α_{gb}	
	300°C	550°C
SG	0.80	0.70
GN	0.83	0.70
SPR	0.90	0.72

TABLE 3. Microhardness and Fracture Toughness of Samples of the Ceramic Ce_{0.8}Y_{0.2}O_{2-δ}

Method of sample preparation	Vickers hardness, GPa	Fracture toughness, MPa · m ^{1/2}
SG	11.56	2.29
GN	8.78	1.88
SPR	6.00	1.73

8.78 and 6.00 GPa, respectively, for the GN and SRP methods and the fracture toughness 1.88 and 1.73 MPa · m^{1/2}, which is confirmed by photographs of indenter prints displayed in Fig. 6 and is associated with the densest packing of atoms due to the smallest grain size.

The measurements of the microhardness and fracture toughness of the ceramic Ce_{0.8}Y_{0.2}O_{2-δ} are consistent with the experimental data presented in [21, 27].

CONCLUSIONS

The ceramics Ce_{0.8}Y_{0.2}O_{2-δ} were obtained by three methods — SG, GN, and SPR with a sintering at 1350°C for the SG method and 1500°C for the rest. It was shown that the cubic fluorite structure belonging to CeO₂ dominates in all samples. It was established by means of impedance spectroscopy that ceramics obtained by the SG method have the highest electrical conductivity, reaching 5.37 mS/cm at 550°C and the lowest activation energy (0.83 eV), which is due to the highest density of the material — 6.51 g/cm³ and the smallest grain size 0.4 μm, which provides the least resis-

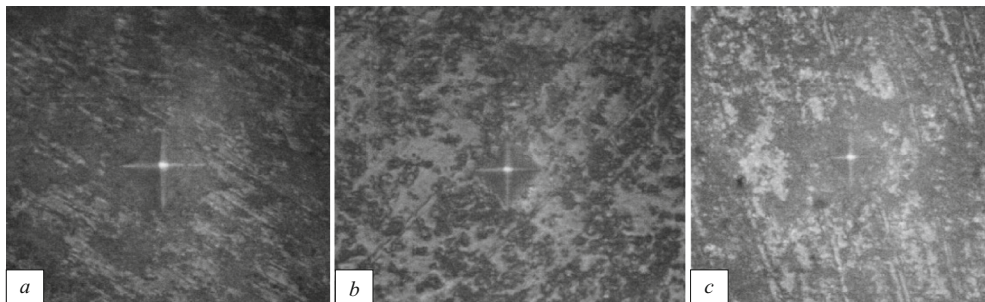


Fig. 6. Indenter Imprints in samples of the ceramic system Ce_{0.8}Y_{0.2}O_{2-δ} obtained by different methods: a) SPR; b) GN; c) SG.

tance along the grain boundaries in comparison with the GN and SPR methods, which also effects the highest hardness and fracture toughness.

This work was financially supported by the competitive part of the state assignment for the creation and development of laboratories, project No. FZWG-2020-0032 (2019-1569), using the equipment of the Center for Collective Use "Technologies and Materials of the National Research University" BelSU with financial support from the Ministry of Science and Higher Education of the Russian Federation within the context of the agreement No. 075-15-2021-690 (unique project identifier RF-2296.61321X0030).

REFERENCES

1. L. Fan, C. Wang, M. Chen, and B. Zhu, "Recent development of ceria-based (nano) composite materials for low temperature ceramic fuel cells and electrolyte-free fuel cells," *J. Power Sources*, **234**, 154 – 174 (2013).
2. Lingyao Li, Bin Zhu, Jing Zhang, et al., "Electrical properties of nanocube CeO₂ in advanced solid oxide fuel cells," *Int. J. Hydrogen Energy*, **43**, 12909 – 12916 (2018).
3. Zh. Gao, L. V. MoGni, E. C. Miller, et al., "A perspective on low-temperature solid oxide fuel cells," *Energy Envir. Sci.*, **9**(5), 1602 – 1644 (2016).
4. J. Zhang, Ch. Lenser, N. H. Menzler, and O. Guillon, "Comparison of solid oxide fuel cell (SOFC) electrolyte materials for operation at 500°C," *Solid State Ionics*, **344**, 115138 (2020).
5. Z. Liu, D. Ding, M. Liu, et al., "High-performance, ceria-based solid oxide fuel cells fabricated at low temperatures," *J. Power Sources*, **241**, 454 – 459 (2013). DOI: 10.1016/j.jpowsour.2013.04.130
6. B. C. H. Steele, "Appraisal of Ce_{1-y}Gd_yO_{2-y/2} electrolytes for IT-SOFC operation at 500°C," *Solid State Ionics*, **129**, 95 – 110 (2000).
7. R. Doshi, V. L. Richards, D. J. Carter, et al., "Development of solid-oxide fuel cells that operate at 500°C," *J. Electrochem. Soc.*, **146**(4), 1273 – 1278 (1999).
8. S. K. Tadoroko, TC Porfirio, R. Muccillo, and E. N. S. Muccillo, "Synthesis, sintering and impedance spectroscopy of 8 mol % yttria-doped ceria solid electrolyte," *J. Power Sources*, **130**, 15 – 21 (2004).
9. Q. Shi, J. Chen, Yu. Xing, et al. "Semiconductor heterostructure StTiO₃/CeO₂ electrolyte membrane fuel cells," *J. Electrochem. Soc.*, **167**, 054504 (2020).
10. E. L. Brosha, R. Mukundan, D. R. Brown, et al., "Development of ceramic mixed potential sensors for automotive applications," *Solid State Ionics*, **148**, 61 – 69 (2002).
11. U. Nigge, H. D. Wiemhofer, E. W. J. Romer, et al. "Composites of Ce_{0.8}Gd_{0.2}O_{1.9} and Gd_{0.7}Ca_{0.3}CoO₃ as oxygen permeable membranes for exhaust gas sensor," *Solid State Ionics*, **146**(1 – 2), 163 (2002).
12. A. Hashimoto, T. Hibino, M. A Sano, "Fuel-cell-type sensor for detection of carbon monoxide in reformed gases," *Electrochem. Solid State Lett.*, **5**(2), (2002).
13. M. Melchionna and P. Fornasiero, "The role of ceria-based nanostructured materials in energy applications," *Materials Today*, **17**(7), 349 – 357 (2014).
14. D. He, H. Hao, D. Chen, et al., "Synthesis and application of rare-earth elements (Gd, Sm, and Nd) doped ceria-based solid solutions for methyl mercaptan catalytic decomposition," *Catalysis Today*, **281**(3), 559 – 565 (2017).
15. A. Vita, "Catalytic applications of CeO₂-based materials," *Catalysts*, **10**, 576 (2020). URL: <https://doi.org/10.3390/catal10050576>
16. D. Nikbin, "Micro SOFCs: why small is beautiful," *Fuel Cell Rev.*, No. 3, 21 – 24 (2006).
17. A. Bieberle-Hutter, D. Beckel, U. Muecke, et al., "Micro-solid oxide fuel cells as battery replacement," *Mst News*, No. 4 – 5, 12 – 15 (2005).
18. A. Bieberle-Hutter, D. Beckel, A. Infortuna, et al., "A micro-solid oxide fuel cell system as battery replacement," *J. Power Sources*, **177**, 123 – 130 (2008). DOI:10.1016/j.jpowsour.2007.10.092.
19. G. Robert, *Micro Fuel Cells for Portable Applications*, European Patent EP 1455409A1.
20. H. Xu, H. Yan, and Z. Chen, "Sintering and electrical properties of Ce_{0.8}Y_{0.2}O_{1.9} powders prepared by citric acid- nitrate low-temperature combustion process," *J. Power Sources*, **163**, 409 – 414 (2006).
21. K. P. Padmasree, R. A. Montalvo-Lozano, S. M. Montemayor, and A. F. Fuentes, "Electrical conduction and dielectric relaxation process in Ce_{0.8}Y_{0.2}O_{1.9} electrolyte system," *J. Alloys Compounds*, **509**, 8584 – 8589 (2011).
22. B. Wang, B. Zhu, S. Yun, et al., "Fast ionic conduction in semiconductor CeO_{2-δ} electrolyte fuel cells," *NPG Asia Mater.*, **11**, 51 (2019).
23. H. Inaba and H. Tagawa, "Ceria-based solid electrolytes," *Solid State Ionics*, **83**, 1 – 16 (1996).
24. A. L. Horovistiz, R. A. Rocha, and E. N. S. Muccillo, "Electrical conductivity and microstructure relationship in ternary systems based on cerium oxide," *Ceram. Int.*, **39**, 5887 – 5892 (2013).
25. P. Ramos-Alvarez, M. E. Villafuerte-Castrejon, G. Gonzalez, et al., "Ceria-based electrolytes with high surface area and improved conductivity for intermediate temperature solid oxide fuel cells," *J. Mater. Sci.*, **52**, 519 – 532 (2017).
26. H. Yoshida, K. Miura, T. Fukui, et al., "Sintering behavior of Ln-doped ceria compounds containing gallia," *J. Power Sources*, **106**, 136 – 141 (2002). URL: [https://doi.org/10.1016/S0378-7753\(01\)01038-2](https://doi.org/10.1016/S0378-7753(01)01038-2)
27. J. Ma, T. S. Zhang, L. B. Kong, et al., "Preparation and characterization of dense Ce_{0.85}Y_{0.15}O_{2-δ} ceramics," *J. Eurp. Ceram. Soc.*, **24**, 2641 – 2648 (2004).
28. R. Gerhardt and A. S. Nowick, "Grain-boundary effect in ceria doped with trivalent cations: I. Electrical measurements," *J. Am. Ceram. Soc.*, **69**(9), 641 – 646 (1986).
29. L. S. Mahmud, A. Muchtar, and M. R. Somalu, "Challenges in fabricating planar solid oxide fuel cells: a review," *Renew. Sustain. Energy Rev.*, **72**, 105 – 116 (2017). URL: <https://doi.org/10.1016/j.rser.2017.01.019>
30. D. H. Prasad, J.-W. Son, B.-K. Kim, et al., "Synthesis of nano-crystalline Ce_{0.9}Gd_{0.1}O_{1.95} electrolyte by novel sol-gel thermolysis process for IT-SOFCs," *J. Eurp. Ceram. Soc.*, **28**(I)(16), 3107 – 3112 (2008). URL: <https://doi.org/10.1016/j.jeurceramsoc.2008.05.021>
31. C. Tian and S.-W. Chan, "Ionic conductivities, sintering temperatures and microstructures of bulk ceramic CeO₂ doped with Y₂O₃," *Solid State Ionics*, **134**, 89 – 102 (2000). URL: [https://doi.org/10.1016/S0167-2738\(00\)00717-7](https://doi.org/10.1016/S0167-2738(00)00717-7)
32. Y.-P. Fu, "Ionic conductivity and mechanical properties of Y₂O₃-doped CeO₂ ceramics synthesis by microwave-induced combustion," *Ceram. Int.*, **35**, 653 – 659 (2009).

33. J. G. Li, Y. Wang, T. Ikegami, and T. Ishigaki, "Densification below 1000°C and grain growth behaviors of yttria doped ceria ceramics," *Solid State Ionics*, **179**, 951 – 954 (2008). URL: <https://doi.org/10.1016/j.ssi.2008.01.053>
34. C. X. Guo, J. X. Wang, C. R. He, and W. G. Wang, "Effect of alumina on the properties of ceria and Scandia co-doped zirconia for electrolyte-supported SOFC," *Ceram. Int.*, **39**, 9575 – 9582 (2013). URL: <http://dx.doi.org/10.1016/j.ceramint.2013.05.076>
35. N. J. Kidner, N. H. Perry, and T. O. Mason, "The brick model revisited: Introducing the nanj-grain composite model," *J. Am. Ceram. Soc.*, **91**(6), 1733 – 1746 (2008). URL: <https://doi.org/10.1111/j.1551-2916.2008.02445.x>
36. C. R. Foschii, D. P. F. Souza, P. I. P. Filho, and J. A. Varela, "AC impedance study of Ni, Fe, Cu, Mn doped ceria stabilized zirconia ceramics," *J. Eurp. Ceram. Soc.*, **21**(1)(9), 1143 – 1150 (2001). URL: [https://doi.org/10.1016/S0955-2219\(00\)00339-3](https://doi.org/10.1016/S0955-2219(00)00339-3)
37. K. Neuhaus, R. Dolle, and H.-D. Wiemhofer, "The effect of transition metal oxide addition on the conductivity of commercially available Gd-doped ceria," *J. Electrochem. Soc.*, **167**, 044507 (2020). URL: <https://iopscience.iop.org/article/10.1149/1945-7111/ab729b/pdf>
38. K. Niihara, R. Morena, and D. P. H. Hasselman, "Evaluation of K_{Ic} of brittle solids by the indentation method with low crack-to-indent rations," *Mater. Sci. Lett.*, No. 1, 13 – 16 (1982).